AGU PUBLICATIONS

Geophysical Research Letters

RESEARCH LETTER
10.1002/2015GL064738

Key Points:
- New method to describe Greenland ice sheet freshwater forcing
- Simplicity enables application to various models and scenarios
- Model results show little impact on Atlantic meridional overturning

Supporting Information:
- Supporting Information S1
- Figure S1
- Data Set S2

Correspondence to:
J. T. M. Lenaerts,
j.lenaerts@uu.nl

Citation:
Lenaerts, J. T. M., D. Le Bars, L. van Kampenhout, M. Vizcaino, E. M. Enderlin, and M. R. van den Broeke (2015), Representing Greenland ice sheet freshwater fluxes in climate models, *Geophys. Res. Lett.*, *42*, 6373–6381, doi:10.1002/2015GL064738.

Received 28 MAY 2015
Accepted 17 JUL 2015
Accepted article online 21 JUL 2015
Published online 6 AUG 2015

Representing Greenland ice sheet freshwater fluxes in climate models

Jan T. M. Lenaerts[1], Dewi Le Bars[1], Leo van Kampenhout[1], Miren Vizcaino[2], Ellyn M. Enderlin[3], and Michiel R. van den Broeke[1]

[1]Institute for Marine and Atmospheric research Utrecht, Utrecht University, Utrecht, Netherlands, [2]Department of Geoscience and Remote Sensing (GRS), Delft University of Technology, Delft, Netherlands, [3]Climate Change Institute & School of Earth and Climate Sciences, University of Maine, Orono, Maine, USA

Abstract Here we present a long-term (1850–2200) best estimate of Greenland ice sheet (GrIS) freshwater runoff that improves spatial detail of runoff locations and temporal resolution. Ice discharge is taken from observations since 2000 and assumed constant in time. Surface meltwater runoff is retrieved from regional climate model output for the recent past and parameterized for the future based on significant correlations between runoff and midtropospheric (500 hPa) summer temperature changes over the GrIS. The simplicity of this approach enables assimilation of meltwater runoff into coupled climate models, which is demonstrated here in a case study with the medium-resolution (1°) Community Earth System Model. The model results suggest that the decrease in Atlantic Meridional Overturning Circulation (AMOC) is dominated by warming of the surface ocean and enhanced GrIS freshwater forcing leads to a slightly enhanced (−1.2 sverdrup in the 21st century) weakening of the AMOC.

1. Introduction

Earth's ice sheets, Greenland (GrIS hereafter) and Antarctica, influence global climate in various ways. Their highly reflective surfaces reduce the Earth's radiation balance [*Flanner et al.*, 2011], and they impact ocean circulation, both directly, by discharging freshwater [*Aagaard and Carmack*, 1989], and indirectly, through their strong control on large-scale atmospheric circulation [*Gong et al.*, 2015]. The volume of ice sheet freshwater forcing (FWF) has increased significantly in the most recent 25 years, both from Antarctica, by enhanced glacier calving and ice shelf melt [*Mouginot et al.*, 2014; *Paolo et al.*, 2015], and from the GrIS, dominated by an increase in surface runoff [*Enderlin et al.*, 2014; *Van Angelen et al.*, 2013a; *Hanna et al.*, 2013a]. This has not only made the ice sheets into major contributors to recent sea level rise [*Rignot et al.*, 2011; *Shepherd et al.*, 2012; *Yi et al.*, 2015; *Hanna et al.*, 2013b] but also altered the freshwater budget of the surrounding oceans and therewith the ocean circulation and ecology [*Bamber et al.*, 2012; *Meredith et al.*, 2010]. The input of cold freshwater limits vertical mixing processes in the upper ocean [*Schmittner et al.*, 2005], which drive the meridional ocean heat transport cells such as the Atlantic Meridional Overturning Circulation (AMOC), which in turn strongly moderate climate in the densely populated midlatitude regions such as western Europe [*Sutton and Hodson*, 2005; *Sutton and Dong*, 2012].

It remains uncertain to what extent GrIS FWF increase has contributed to observed changes in ocean dynamics and recent AMOC weakening [*Rahmstorf et al.*, 2015]. Direct oceanic observations of the AMOC only started in 2004 [*Rayner et al.*, 2011], a period that is too short to separate internal from forced variability [*Roberts et al.*, 2014]. To assess the long-term impact of GrIS FWF on global climate, a coupled ice sheet-ocean-atmosphere model setup is required. However, even state-of-the-art climate models from the most recent Intergovernmental Panel on Climate Change Coupled Model Intercomparison Project Phase 5 (CMIP5) modeling effort fail to realistically represent GrIS surface mass balance (SMB) processes [*Cullather et al.*, 2014] and do not explicitly include FWF from changes in iceberg calving (i.e., ice dynamics). Most models use a mass conservation approach to estimate ice sheet mass change: the mass gained through snowfall at the ice sheet surface is matched by an equivalent mass loss, prescribed as runoff along the ice sheet periphery. Existing assessments of the impact of GrIS FWF on regional and global climate have been limited to low-resolution [*Swingedouw et al.*, 2006; *Mikolajewicz et al.*, 2007; *Ridley et al.*, 2005], intermediate-complexity [*Fichefet*, 2003; *Kuhlbrodt et al.*, 2009] or ocean-only [*Weijer et al.*, 2012; *Den Toom et al.*, 2014] models. Moreover, FWF

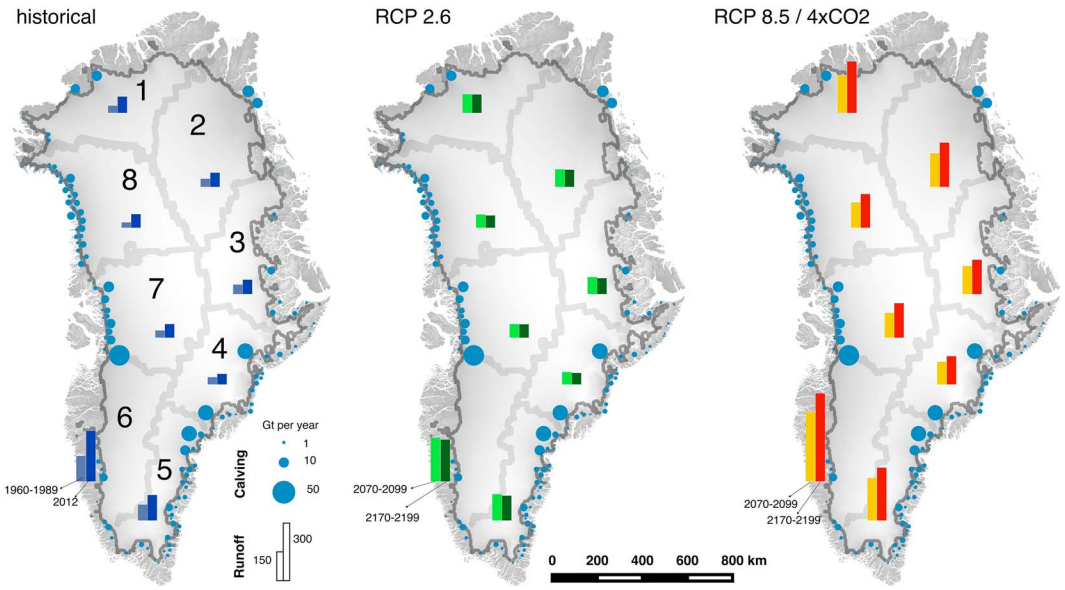

Figure 1. (left) Reconstruction and future evolution of GrIS runoff (bars) and glacier discharge (circles): (middle) RCP2.6 and (right) RCP8.5/4 × CO_2. The background on the maps shows the basin and ice sheet delineation (grey lines) and the Greenland continental extent derived from the Greenland Ice Mapping Project (GIMP) data set [*Howat et al.*, 2014].

prescribed to these models is usually highly idealized, i.e., without interannual or seasonal variability and uniform along the ice sheet margins [*Jungclaus et al.*, 2006; *Swingedouw et al.*, 2014].

Here we use a combination of observed GrIS ice discharge and simulated surface runoff, the latter regressed to changes in midtropospheric temperatures [*Fettweis et al.*, 2013a], to construct a best estimate of past, present and future Greenland ice sheet freshwater forcing (1850–2200) that includes the significant seasonal to interannual variations in runoff [*Van As et al.*, 2014] and spatial variations in both runoff and glacier discharge [*Moon et al.*, 2014]. Next, we apply this freshwater forcing to a CMIP6 generation, atmosphere-ocean coupled climate model for two climate change scenarios, Representative Concentration Pathways 2.6 (RCP2.6) and RCP8.5. Section 2 presents the FWF and the climate model, section 3 discusses the results, and section 4 gives the conclusions.

2. Methodology

2.1. Setup of Freshwater Forcing

The freshwater flux from the GrIS consists of ice flow over the grounding line (solid ice discharge) on the one hand and supraglacial, subglacial, and englacial runoff of liquid water on the other. GrIS ice discharge is constructed following *Enderlin et al.* [2014], who used remote sensing techniques to estimate discharge from 178 individual GrIS glaciers for the period 2000–2012 (Figure 1). In this study we focus on variability in runoff and assume solid ice discharge to be constant in time, which is motivated by relatively small intra-annual variations in glacier velocities [*Moon et al.*, 2014], the large and spatially asynchronous interannual variations in ice discharge in the 2000–2012 period [*Enderlin et al.*, 2014], and the relatively short time period of observations, which prevents assessment of long-term trends [*Wouters et al.*, 2013]. Although GrIS ice discharge estimates for 1996 were ~30 Gt yr^{-1} lower than the 2000 estimates [*Rignot et al.*, 2008], we cannot assess whether the 1996 values are representative of long-term mean iceberg calving rates of the preceding decades [*Jiang et al.*, 2010]. Figure 1 shows that the highest discharge values are found in west Greenland, with Jakobshavn Glacier discharging ~53 Gt yr^{-1}, and southeastern Greenland, with several glaciers that discharge >20 Gt yr^{-1} [*Enderlin et al.*, 2014].

To reconstruct past, present, and future GrIS freshwater forcing originating from meltwater runoff, we use output of the high-resolution (~11 km) regional atmospheric climate model RACMO, version 2.1 (RACMO2 hereafter). RACMO2, forced by ERA-Interim fields at its lateral boundaries (RACMO2-ERAI, 1960–2012), realistically simulates present-day GrIS climate [*Ettema et al.*, 2010; *Lenaerts et al.*, 2014] and SMB [*Van Angelen et al.*, 2013a]. To simulate a future warming scenario, RACMO2 was forced by atmospheric fields of the general

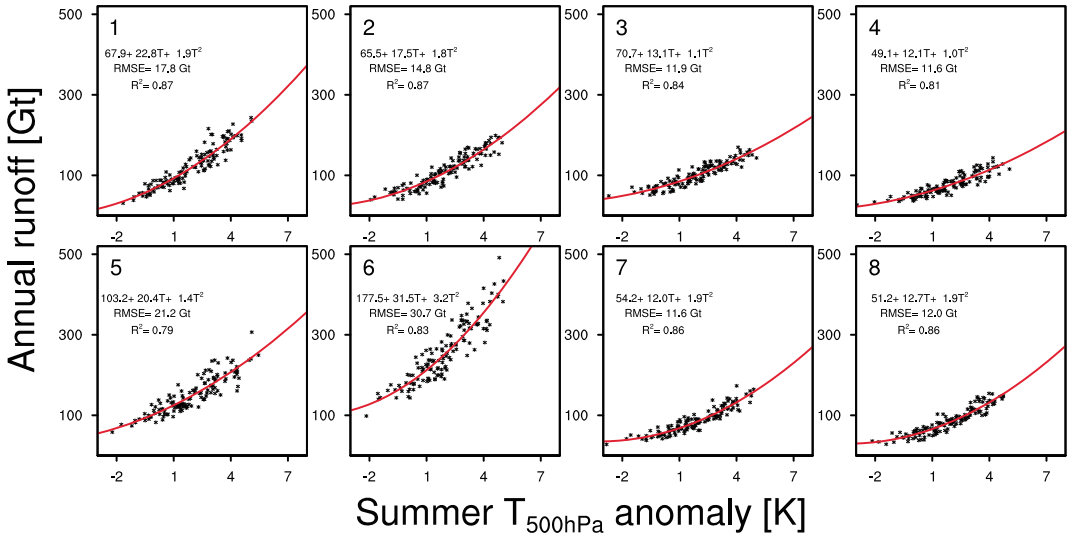

Figure 2. GrIS basin integrated surface runoff versus 500 hPa temperature anomalies according to RACMO2-HG (1970–2098). The fitted second-order polynomials are drawn with red lines. Basin definitions are shown in Figure 1.

circulation climate model HadGEM2-ES (RACMO2-HG, 1971–2100). RACMO2-HG was forced by the midway future climate change scenario RCP4.5. We refer to *Van Angelen et al.* [2013a, 2013b] for a detailed evaluation and analysis of RACMO2-ERAI and RACMO2-HG, respectively.

To represent the strong spatial variations in meltwater runoff over the GrIS [*Van Angelen et al.*, 2013a], we subdivide the GrIS in eight basins (Data Set S1 in the supporting information, [*Wouters et al.*, 2008]) and calculate past runoff from RACMO2-ERAI (1960–2012) for each basin. Note that we also include runoff from the melting of seasonal snow covering the tundra area that surrounds the GrIS in our calculations. Prior to 1960, we lack data on surface runoff, especially on the glacier catchment scale [*Box*, 2013]. Therefore, we assume that GrIS runoff in the period 1960–1989 was representative for the years 1850–1959, in line with the results from *Box* [2013], and that the 1960–1989 time series of annual runoff obeys a normal distribution.

To deduce a general parameterization for future GrIS runoff, we use the RACMO2-HG output. RACMO2-HG not only realistically represents the present-day climate of the GrIS, it also considers the important buffering effect of meltwater refreezing and retention in liquid form within the GrIS snowpack [*Van Angelen et al.*, 2013b; *Forster et al.*, 2014]. Next we correlate the RACMO2-HG annual surface runoff to simulated midtropospheric (500 hPa) summer (June-July-August) temperature anomalies (with respect to the period 1971–2000 [*Fettweis et al.*, 2013b]), for each of the eight basins (referred to as T500). The factors of the polynomial fits are given in Data Set S2. T500 is a commonly used proxy for the large-scale atmospheric state, not significantly affected by local surface processes, and readily available from all climate model output archives. Figure 2 shows a significant correlation between runoff and T500 for all basins, with the squared correlation coefficient (R^2) and the root-mean-squared error >0.8 and < 30 Gt for all basins, respectively. While RACMO2-HG simulates a 21st century T500 increase of ~5 K within each basin, the surface runoff response to this warming strongly varies from basin to basin. The strongest nonlinear response of runoff is found in northern and northeastern Greenland (basins 1 and 2) and, in particular, southwestern Greenland (basin 6). This is in agreement with *Tedesco and Fettweis* [2012], who consistently found the highest sensitivity of surface runoff to near-surface temperature increase in the northeast and southwest in various climate models and climate change scenarios. These regions are most sensitive to future warming because they have the highest relative coverage of ablation zone, where meltwater runs off directly. In other regions, a higher fraction of meltwater refreezes, buffering the runoff.

Although we only use a single regional climate model simulation to derive the robust, stronger-than-linear relation between T500 and runoff, it appears to be general for a wide range of scenarios [*Tedesco and Fettweis*, 2012; *Fettweis et al.*, 2013b]. It allows us to determine second-order polynomials for each basin (Figure 2), which can then be applied to a T500 time series from any existing climate model in order to construct a GrIS runoff time series. Here we use T500 from the Community Climate System Model version 4 simulation,

spanning until 2200 [*Meehl et al.*, 2013], driven by two differing CMIP5 climate change scenarios (Figure S1). In the RCP2.6 scenario, global emissions are strongly suppressed in the 21st century, leading to a modest warming over the GrIS until 2100 (~2 K), and a gradual cooling toward present-day temperatures afterward. In the RCP8.5/4 × CO_2 scenario, contemporary emission increases are sustained, strongly increasing atmospheric temperatures, especially above Greenland (~5 K warmer in 2100). From the year ~2120 onward, the original RCP8.5 scenario is modified: greenhouse gas emissions are suppressed, and atmospheric CO_2 concentrations level off at 4 times the preindustrial levels (~1300 ppmv), leading to a continuously high GrIS runoff until 2200.

We choose these future greenhouse gas scenarios because we are not only interested in the response of the AMOC to a future increase in GrIS runoff but also if/how the AMOC recovers when GrIS runoff stabilizes at either near present-day values (RCP2.6) or considerably higher values under strong warming conditions (RCP8.5/4 × CO_2).

Apart from considering spatial and interannual variability in GrIS runoff, we also introduce a seasonal cycle at monthly time resolution, with a runoff peak in summer and little to no runoff in winter. This seasonal cycle is determined from the mean RACMO2-ERAI seasonal cycle for the period 1960–2012, which is then normalized and scaled with the annual runoff for each individual year in the final 1850–2200 time series.

2.2. Climate Model Simulations

Here we use the coupled land-atmosphere-ocean climate model Community Earth System Model (CESM, version 1.1.2) with a horizontal resolution of ~1°, which has been set up similarly to the CESM simulations for CMIP5 [*Meehl et al.*, 2013] but is updated to a more recent model version, similar to the CESM Large Ensemble [*Kay et al.*, 2014] but with a different ozone forcing [*Marsh et al.*, 2013]. The ocean in CESM, simulated by the Parallel Ocean Program ocean model, is initialized after running a control simulation with constant preindustrial forcing for 1500 years, similar to the CESM-Large Ensemble [*Kay et al.*, 2014], to ensure that the deep ocean is in equilibrium with the preindustrial climate. Next, CESM is used to simulate six different scenarios: two historical simulations (1850–2005), one with (FWF-hist) and one without (NOFWF-hist) our reconstructed FWF, and four future simulations, forced by the RCP2.6 and RCP8.5/4 × CO_2 future emission scenarios, and each with (FWF) and without (NOFWF) the FWF corresponding to the same scenario (see section 2.1). In the NOFWF simulations, we allow CESM to calculate its own ice sheet freshwater forcing according to the original formulation. This means that CESM generates liquid freshwater through surface runoff, whereas solid ice discharge, in absence of ice dynamics, is set equal to the precipitation that falls on the ice sheet and is not stored in the snow model; this amount is then instantaneously discharged into the nearest ocean grid point. In the FWF simulations, we assimilate our best estimate of GrIS freshwater forcing to the ocean grid points fringing the ice sheet. For solid ice discharge, we assign each glacier discharge flux to the nearest ocean grid point. At each 15 min model time step, liquid freshwater (i.e., runoff) is distributed evenly in all grid cells along each individual basin, and assimilated into CESM. Although it is not part of this study, note that we also assimilate FWF from the Antarctic ice sheet on subice sheet scale, following *Depoorter et al.* [2013].

3. Results

The spatial and temporal variability of the reconstructed GrIS runoff are depicted in Figures 1 and 3a, respectively. Before 1990, the GrIS freshwater forcing generated internally by CESM (1041 ± 78 Gt yr^{-1} in NOFWF-hist) compares with the assimilated GrIS FWF within the uncertainties (965 ± 31 Gt yr^{-1} in FWF-hist). This confirms that CESM is able to reasonably resolve contemporary GrIS climate, although the slightly higher FWF in CESM is related to an overestimation of solid precipitation on the GrIS in the model. RACMO2-ERAI derived runoff varies between 30 Gt yr^{-1} in the northernmost basins to 130 Gt yr^{-1} in basin 6 (southwest Greenland). From the 1990s onward, our GrIS FWF estimates start to diverge from the CESM FWF estimates (Figure 3a). In 2012, when the GrIS experienced an exceptionally warm summer, runoff was particularly high (>200% higher than the 1960–1989 mean) in the basins in west Greenland (basins 1, 6, 7, and 8) and only marginally higher than normal in east Greenland. The 2012 runoff peak was driven by anomalously strong heat and moisture advection toward west Greenland, enhancing surface melt and runoff [*Fettweis et al.*, 2013a; *Neff et al.*, 2014; *Hanna et al.*, 2014].

The assimilated GrIS FWF in 2012 (equal to 1347 Gt) is the highest of the historical period. Our results indicate that annual GrIS FWF at the end of the 21st century will typically exceed that of 2012, both in the RCP2.6 scenario (1366 ± 97 Gt yr^{-1} in 2070–2099) but particularly in the RCP8.5/4 × CO_2 scenario (1994 ± 201 Gt yr^{-1}).

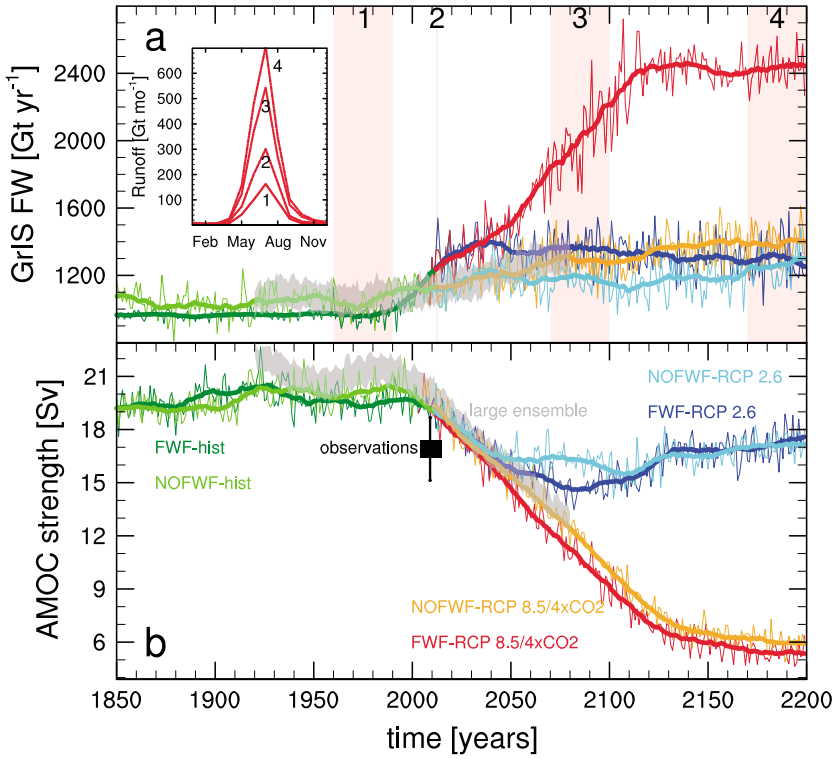

Figure 3. Time series of annual (thin lines) and 20 year running means (thick lines) of (a) GrIS freshwater forcing and (b) AMOC strength (defined as the maximal meridional stream function at 26°N and below 500 m depth) according to the different scenarios. The inset shows the seasonal cycle of reconstructed runoff in four periods, numbered chronologically and shown by the grey vertical bars in Figure 3a. The CESM-Large Ensemble mean ± standard deviation of the 30 members is represented by the grey band in both graphs. The black whisker shows the mean ± one standard deviation of the annual AMOC observations along the RAPID array in the period 2004–2014 [*McCarthy et al.*, 2015].

The highest relative runoff increase in both scenarios is found in southwest and east Greenland (Figure 1), the regions with the highest sensitivity of runoff to summer temperature increase (Figure 2). The resulting surface runoff anomaly in 2100 (~950 Gt yr^{-1} higher than in 2000) compares well with the recent estimate of ~950 Gt yr^{-1} [*van den Berk and Drijfhout*, 2014] and is within the range of regional climate model output driven by various CMIP5 models (600–1200 Gt yr^{-1} [*Fettweis et al.*, 2013b; *Van Angelen et al.*, 2013b]).

In the RCP2.6 scenario, the runoff increase levels off after the year ~2050 and runoff even slightly decreases throughout the remainder of the 21st and 22nd centuries. In the RCP8.5/4 × CO_2 scenario, runoff steadily increases until ~2120, after which GrIS summer temperatures do not increase anymore, and FWF stabilizes at 2426 ± 102 Gt yr^{-1} in the period 2170–2199. Noteworthy is the much higher interannual variability of freshwater forcing in the RCP8.5/4×CO_2 scenario relative to the RCP2.6 scenario, in response to higher interannual melt variations in a warmer climate [*Fyke et al.*, 2014]. Since we impose a seasonal cycle to the runoff, the summer freshwater forcing becomes very strong; for instance, the ~700 Gt runoff in July (inset in Figure 3a) is equivalent to ~0.27 Sv (sverdrup), which approximates typical idealized GrIS freshwater forcing used in GrIS hosing studies (0.1–0.5 Sv [*Weijer et al.*, 2012]). In contrast, none of the NOFWF scenarios show a strong increase of GrIS FWF (Figure 3a) into the future, because CESM, similar to other CMIP5 climate models, does not allow the Greenland ice sheet to change mass in response to increasing temperatures. The slight freshwater increase in the 21st century in the NOFWF simulations is caused by enhanced precipitation on the GrIS and by melting the shallow model snowpack [*Vizcaíno et al.*, 2013] along the GrIS margins.

Next we examine the response of the simulated AMOC to predicted GrIS FWF (Figure 3b). In the historical period, the AMOC strength is comparable between the NOFWF and FWF runs (19.7 ± 0.8 Sv in 1850–2005), somewhat larger than observational estimates. Our simulations show a 1–2 Sv weaker AMOC compared to the CESM Large Ensemble of 30 members [*Kay et al.*, 2014] and are more in line with the observed AMOC strength along the RAPID array (16.9 ± 1.8 Sv [*McCarthy et al.*, 2015]). The difference in AMOC strength between our

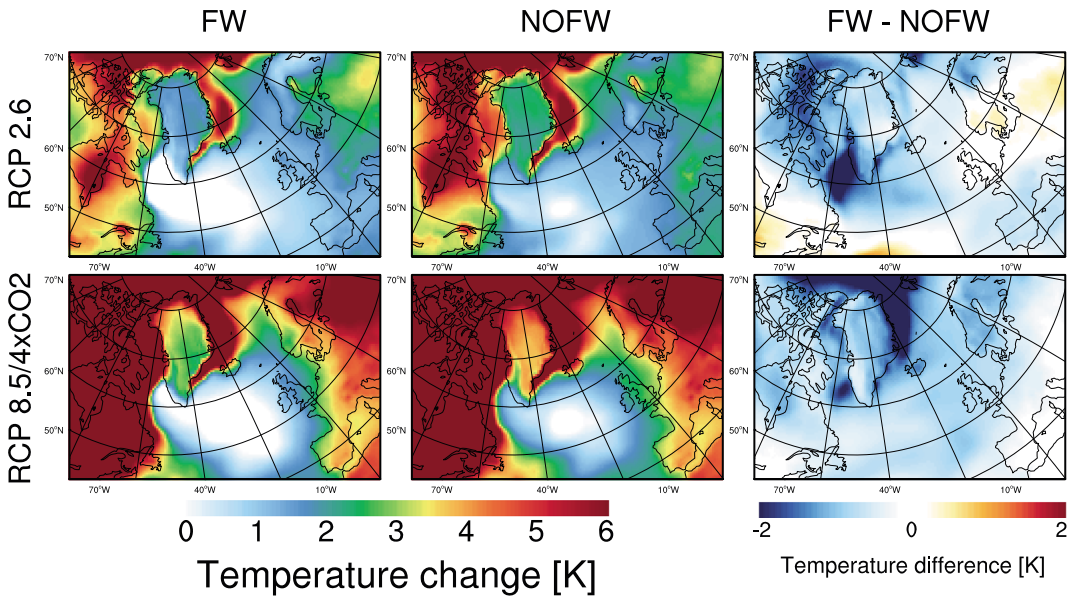

Figure 4. (left and middle columns) Two meter air temperature change (K) between 1960–1989 (period 1 in Figure 3a) and 2070–2099 (period 3 in Figure 3a) for the four future simulations and (right) the differences between FWF and NOFWF for both scenarios.

results and the CESM Large Ensemble is not explained by differing GrIS FWF forcing (Figure 3a) but could be due to differences in the ozone forcing [*Kay et al.*, 2014].

From the late 1990s onward, all simulations show a linear decrease of annual mean AMOC strength. The decline slows down after 2050 in RCP2.6 but continues in RCP8.5/4 × CO_2 until ~2130. The small differences between the FWF and NOFWF simulations in both scenarios indicate that the rate of AMOC slowdown is not greatly/strongly affected by enhanced GrIS FWF but is dominated by ocean surface warming, which increases ocean stratification and reduces vertical mixing. The AMOC slowdown occurs slightly, but significantly (95% confidence interval) faster in the FWF simulations; the AMOC decreases in the 21st century with 112 ± 2 mSv yr^{-1} in the FWF-RCP8.5/4 × CO_2 simulation and 100 ± 2 mSv yr^{-1} in NOFWF-RCP8.5/4 × CO_2. Consequently, the 12 Sv AMOC level is reached 10 years earlier in FWF-RCP8.5 (2074 versus 2084) and the 7 Sv level 11 years earlier (2122 versus 2133). After stabilizing CO_2 levels (around 2130), AMOC quickly stabilizes as well to a shallow AMOC cell reaching a depth of 1500 m compared to 3000 m in the historical simulations. In the RCP2.6 scenario, the AMOC partly recovers after ~2040 in the NOFWF simulation, whereas AMOC keeps decreasing in the FWF simulation until ~2080, before also partly recovering in the 22nd century and reaching the same levels as NOFWF in ~2100.

The largest impact of GrIS FWF on the AMOC is simulated at the end of the 21st century. Since it is hypothesized that AMOC weakening increases the potential of cold winters in western Europe [*Blaker et al.*, 2014; *Bryden et al.*, 2014], we analyze the impact of additional GrIS FWF on wintertime (December-January-February) near-surface (2 m) air temperature changes around Greenland, in the Atlantic Ocean, and western Europe in the period 2060–2089, relative to the present day (Figure 4). In all scenarios, we see markedly different patterns of near-surface temperature change, with the highest (>6 K) increase in the high-latitude Arctic, as well as along the coasts of Greenland, which are sea ice-covered areas in the present day but projected to be sea ice free in the second half of this century, even in winter. Much smaller temperature increases, with even some areas of temperature decrease, are found over the Atlantic Ocean southeast of Greenland, in the area of most vigorous deep water formation. In this region, future AMOC weakening leads to less oceanic heat transport across the Atlantic and a regional decrease of surface temperatures that can offset the overall global warming signal, as may have been observed in the twentieth century [*Rahmstorf et al.*, 2015]. The overall warming patterns are qualitatively similar, but amplified in RCP8.5/4 × CO_2 compared to RCP2.6. If we then compare the FWF and NOFWF experiments, we see an enhanced cooling signal in the Atlantic Ocean, and less warming (~1–2 K) over Greenland itself and over parts of western Europe. We find similar patterns in spring and less prominently in summer and autumn. These results suggest that enhanced GrIS freshwater forcing, through

a slightly and temporary (~10 years) enhanced AMOC weakening, reduces future warming in the Atlantic Ocean. This mechanism might not only temporarily reduce future GrIS melting [*Vizcaíno et al.*, 2008] but could also affect winter climate of western Europe.

4. Conclusions

We present a method to include past, present, and future GrIS FWF in coupled climate models, to overcome their limited ability to directly simulate ice sheet FWF. Past and present solid ice discharge and runoff are inferred from observations and regional climate model simulations, respectively. For future runoff, we use robust correlations between GrIS summer temperatures at 500 hPa and annual runoff at drainage basin scale.

The calculated future GrIS FWF is associated with very large uncertainties. First, the evolution of GrIS solid ice discharge is highly uncertain, and we decided to keep this source of FWF constant rather than extrapolating recently observed trends. A technique relating ice discharge to surface runoff [*Bamber et al.*, 2012] might be appropriate for decadal projections but is likely less relevant for multicentury projections as presented here [*Vizcaíno et al.*, 2015; *Goelzer et al.*, 2013]. We showed that runoff is highly correlated to midtroposphere temperature; although this relation appears to be general in climate model projections [*Fettweis et al.*, 2013b], these relations are also associated with model and scenario inherent uncertainties. For example, the T500 anomalies used for our polynomial fits do not exceed 6 K, while the RCP8.5/4×CO_2 yields higher-temperature anomalies. Moreover, our method does not consider changes in GrIS topography or extent and their impact on GrIS FWF. These effects, however, appear to be overshadowed by the direct impact of atmospheric warming, especially in strong warming scenarios [*Fürst et al.*, 2015; *Vizcaíno et al.*, 2015].

This method offers high temporal (daily) and spatial (glacier/drainage basin) detail and is simple to implement; it can be applied in every climate model, regardless of resolution or scenario, to study the impact of GrIS FWF. A community-based model intercomparison project (AMOCMIP) is currently ongoing, in which this method, driven by the CMIP5 mean T500 change, is applied to several state-of-the-art climate models.

Here we apply our FWF method to the Community Earth System Model (CESM). Our model output suggests that even for a strong warming scenario, enhanced GrIS FWF advances the timing of AMOC weakening but that the overall impact on AMOC stability is small. This finding agrees with existing model assessments [*Swingedouw et al.*, 2014]. In the CMIP5 multimodel ensemble, all models show a weakening of the AMOC in the 21st century [*Weaver et al.*, 2012], while none of these models allows for GrIS melting in the future. In CMIP5, AMOC weakening is dominated by ocean surface warming and sea ice melting in the North Atlantic [*Jahn et al.*, 2012]; in this group of models, CESM seems to be the most sensitive.

With its medium-coarse resolution of ~1°, the current run with CESM does not explicitly resolve ocean eddies. Ocean resolution determines the pathways of freshwater and influences the transient response of the AMOC to additional freshwater flux around Greenland [*Weijer et al.*, 2012]. A forthcoming study will analyze the output of an eddy permitting and coupled version of the CESM (horizontal resolution of ~0.1°), forced with the same GrIS FWF as the medium-resolution CESM presented here.

Acknowledgments

This study is funded by Utrecht University through its strategic theme Sustainability, sub-theme Water, Climate and Ecosystems. Jan Lenaerts acknowledges support from NWO ALW through its Innovational Research Incentives Scheme Veni. Climate simulations were partly performed on SurfSARA HPC systems, with support from NWO Exacte Wetenschappen.

The Editor thanks Xavier Fettweis and two anonymous reviewers for their assistance in evaluating this paper.

References

Aagaard, K., and E. C. Carmack (1989), The role of sea ice and other fresh water in the Arctic circulation, *J. Geophys. Res.*, *94*(C10), 14,485–14,498.

Bamber, J., M. Van Den Broeke, J. Ettema, J. Lenaerts, and E. Rignot (2012), Recent large increases in freshwater fluxes from Greenland into the North Atlantic, *Geophys. Res. Lett.*, *39*, L19501, doi:10.1029/2012GL052552.

Blaker, A. T., J. J.-M. Hirschi, G. McCarthy, B. Sinha, S. Taws, R. Marsh, A. Coward, and B. de Cuevas (2014), Historical analogues of the recent extreme minima observed in the Atlantic meridional overturning circulation at 26°N, *Clim. Dyn.*, *44*(1–2), 457–473.

Box, J. E. (2013), Greenland ice sheet mass balance reconstruction. Part II: Surface mass balance (1840–2010), *J. Clim.*, *26*(18), 6974–6989, doi:10.1175/JCLI-D-12-00518.1.

Bryden, H. L., B. A. King, G. D. McCarthy, and E. L. McDonagh (2014), Impact of a 30% reduction in Atlantic meridional overturning during 2009–2010, *Ocean Sci.*, *10*(4), 683–691.

Cullather, R. I., S. M. Nowicki, B. Zhao, and M. J. Suarez (2014), Evaluation of the surface representation of the Greenland ice sheet in a general circulation model, *J. Clim.*, *27*, 4835–4856, doi:10.1175/JCLI-D-13-00635.1.

Den Toom, M., H. A. Dijkstra, W. Weijer, M. W. Hecht, M. E. Maltrud, and E. van Sebille (2014), Response of a strongly eddying global ocean to North Atlantic freshwater perturbations, *J. Phys. Oceanogr.*, *44*(2), 464–481, doi:10.1175/JPO-D-12-0155.1.

Depoorter, M. A., J. L. Bamber, J. A. Griggs, J. T. M. Lenaerts, S. R. M. Ligtenberg, M. R. van den Broeke, and G. Moholdt (2013), Calving fluxes and basal melt rates of Antarctic ice shelves., *Nature*, *502*(7469), 89–92, doi:10.1038/nature12567.

Enderlin, E. M., I. M. Howat, S. Jeong, M. J. Noh, J. H. Van Angelen, and M. R. Van Den Broeke (2014), An improved mass budget for the Greenland ice sheet, *Geophys. Res. Lett.*, *41*, 866–872, doi:10.1002/2013GL059010.

Ettema, J., M. R. van den Broeke, E. van Meijgaard, and W. J. van de Berg (2010), Climate of the Greenland ice sheet using a high-resolution climate model—Part 1: Evaluation, *Cryosphere*, *4*(2), 511–527, doi:10.5194/tc-4-511-2010.

Fettweis, X., E. Hanna, C. Lang, a. Belleflamme, M. Erpicum, and H. Gallée (2013a), Brief communication "Important role of the mid-tropospheric atmospheric circulation in the recent surface melt increase over the Greenland ice sheet", *Cryosphere*, *7*(1), 241–248, doi:10.5194/tc-7-241-2013.

Fettweis, X., B. Franco, M. Tedesco, J. H. van Angelen, J. T. M. Lenaerts, M. R. van den Broeke, and H. Gallée (2013b), Estimating the Greenland ice sheet surface mass balance contribution to future sea level rise using the regional atmospheric climate model MAR, *Cryosphere*, *7*(2), 469–489.

Fichefet, T. (2003), Implications of changes in freshwater flux from the Greenland ice sheet for the climate of the 21st century, *Geophys. Res. Lett.*, *30*(17), 1911, doi:10.1029/2003GL017826.

Flanner, M. G., K. M. Shell, M. Barlage, D. K. Perovich, and M. A. Tschudi (2011), Radiative forcing and albedo feedback from the Northern Hemisphere cryosphere between 1979 and 2008, *Nat. Geosci.*, *4*(3), 151–155, doi:10.1038/ngeo1062.

Forster, R. R., et al. (2014), Extensive liquid meltwater storage in firn within the Greenland ice sheet, *Nat. Geosci.*, *7*(2), 1–4, doi:10.1038/ngeo2043.

Fürst, J. J., H. Goelzer, and P. Huybrechts (2015), Ice-dynamic projections of the Greenland ice sheet in response to atmospheric and oceanic warming, *Cryosphere*, *9*(3), 1039–1062.

Fyke, J. G., M. Vizcaíno, W. Lipscomb, and S. Price (2014), Future climate warming increases Greenland ice sheet surface mass balance variability, *Geophys. Res. Lett.*, *41*, 470–475, doi:10.1002/2013GL058172.

Goelzer, H., P. Huybrechts, J. J. Fürst, F. M. Nick, M. L. Andersen, T. L. Edwards, X. Fettweis, A. J. Payne, and S. Shannon (2013), Sensitivity of Greenland ice sheet projections to model formulations, *J. Glaciol.*, *59*(216), 733–749, doi:10.3189/2013JoG12J182.

Gong, X., X. Zhang, G. Lohmann, W. Wei, X. Zhang, and M. Pfeiffer (2015), Higher Laurentide and Greenland ice sheets strengthen the North Atlantic ocean circulation, *Clim. Dyn.*, *45*(1–2), 139–150.

Hanna, E., J. M. Jones, J. Cappelen, S. H. Mernild, L. Wood, K. Steffen, and P. Huybrechts (2013a), The influence of North Atlantic atmospheric and oceanic forcing effects on 1900–2010 Greenland summer climate and ice melt/runoff, *Int. J. Climatol.*, *33*(4), 862–880.

Hanna, E., et al. (2013b), Ice-sheet mass balance and climate change, *Nature*, *498*(7452), 51–59.

Hanna, E., X. Fettweis, S. H. Mernild, J. Cappelen, M. H. Ribergaard, C. A. Shuman, K. Steffen, L. Wood, and T. L. Mote (2014), Atmospheric and oceanic climate forcing of the exceptional Greenland ice sheet surface melt in summer 2012, *Int. J. Climatol.*, *34*(4), 1022–1037.

Howat, I. M., A. Negrete, and B. E. Smith (2014), The Greenland Ice Mapping Project (GIMP) land classification and surface elevation data sets, *Cryosphere*, *8*(4), 1509–1518, doi:10.5194/tc-8-1509-2014.

Jahn, A., et al. (2012), Late-twentieth-century simulation of arctic sea ice and ocean properties in the CCSM4, *J. Clim.*, *25*(5), 1431–1452, doi:10.1175/JCLI-D-11-00201.1.

Jiang, Y., T. H. Dixon, and S. Wdowinski (2010), Accelerating uplift in the North Atlantic region as an indicator of ice loss, *Nat. Geosci.*, *3*(6), 404–407.

Jungclaus, J. H., H. Haak, M. Esch, E. Roeckner, and J. Marotzke (2006), Will Greenland melting halt the thermohaline circulation?, *Geophys. Res. Lett.*, *33*, L17708, doi:10.1029/2006GL026815.

Kay, J. E., C. Deser, and A. S. Phillips (2014), The Community Earth System Model (CESM) large ensemble project: A community resource for studying climate change in the presence of internal climate variability, *Bull. Am. Meteorol. Soc.*, *96*, 283–296, doi:10.1175/BAMS-D-14-00017.1.

Kuhlbrodt, T., et al. (2009), An integrated assessment of changes in the thermohaline circulation, *Clim. Change*, *96*(4), 489–537, doi:10.1007/s10584-009-9561-y.

Lenaerts, J. T. M., C. J. P. P. Smeets, K. Nishimura, M. Eijkelboom, W. Boot, M. R. van den Broeke, and W. J. van de Berg (2014), Drifting snow measurements on the Greenland Ice Sheet and their application for model evaluation, *Cryosphere*, *8*(2), 801–814.

Marsh, D. R., M. J. Mills, D. E. Kinnison, J.-F. Lamarque, N. Calvo, and L. M. Polvani (2013), Climate change from 1850 to 2005 simulated in CESM1 (WACCM), *J. Clim.*, *26*(19), 7372–7391.

McCarthy, G., et al. (2015), Measuring the Atlantic Meridional Overturning Circulation at 26°N, *Prog. Oceanogr.*, *130*, 91–111.

Meehl, G. A., et al. (2013), Climate change projections in CESM1 (CAM5) compared to CCSM4, *J. Clim.*, *26*(17), 6287–6308, doi:10.1175/JCLI-D-12-00572.1.

Meredith, M. P., M. I. Wallace, S. E. Stammerjohn, I. A. Renfrew, A. Clarke, H. J. Venables, D. R. Shoosmith, T. Souster, and M. J. Leng (2010), Changes in the freshwater composition of the upper ocean west of the Antarctic Peninsula during the first decade of the 21st century, *Prog. Oceanogr.*, *87*(1–4), 127–143, doi:10.1016/j.pocean.2010.09.019.

Mikolajewicz, U., M. Gröger, E. Maier-Reimer, G. Schurgers, M. Vizcaíno, and A. M. E. Winguth (2007), Long-term effects of anthropogenic CO2 emissions simulated with a complex earth system model, *Clim. Dyn.*, *28*(6), 599–633, doi:10.1007/s00382-006-0204-y.

Moon, T., I. Joughin, B. Smith, M. R. van den Broeke, W. J. van de Berg, B. Noël, and M. Usher (2014), Distinct patterns of seasonal Greenland glacier velocity, *Geophys. Res. Lett.*, *41*, 7209–7216, doi:10.1002/2014GL061836.

Mouginot, J., E. Rignot, and B. Scheuchl (2014), Sustained increase in ice discharge from the Amundsen Sea Embayment, West Antarctica, from 1973 to 2013, *Geophys. Res. Lett.*, *41*, 1576–1584, doi:10.1002/2013GL059069.

Neff, W., G. P. Compo, F. Martin Ralph, and M. D. Shupe (2014), Continental heat anomalies and the extreme melting of the Greenland ice surface in 2012 and 1889, *J. Geophys. Res. Atmos.*, *119*, 6520–6536, doi:10.1002/2014JD021470.

Paolo, F. S., H. a. Fricker, and L. Padman (2015), Volume loss from Antarctic ice shelves is accelerating, *Science*, *348*(6232), 327–331, doi:10.1126/science.aaa0940.

Rahmstorf, S., J. E. Box, G. Feulner, M. E. Mann, A. Robinson, S. Rutherford, and E. J. Schaffernicht (2015), Exceptional twentieth-century slowdown in Atlantic Ocean overturning circulation, *Nat. Clim. Change*, *5*(5), 475–480, doi:10.1038/nclimate2554.

Rayner, D., et al. (2011), Monitoring the Atlantic meridional overturning circulation, *Deep Sea Res. Part II*, *58*(17–18), 1744–1753, doi:10.1016/j.dsr2.2010.10.056.

Ridley, J. K., P. Huybrechts, J. M. Gregory, and J. A. Lowe (2005), Elimination of the Greenland ice sheet in a High CO_2 *Climate*, *J. Clim.*, *18*(17), 3409–3427.

Rignot, E., J. E. Box, E. Burgess, and E. Hanna (2008), Mass balance of the Greenland ice sheet from 1958 to 2007, *Geophys. Res. Lett.*, *35*, L20502, doi:10.1029/2008GL035417.

Rignot, E., I. Velicogna, M. R. Van Den Broeke, a. Monaghan, and J. Lenaerts (2011), Acceleration of the contribution of the Greenland and Antarctic ice sheets to sea level rise, *Geophys. Res. Lett.*, *38*, L05503, doi:10.1029/2011GL046583.

Roberts, C. D., L. Jackson, and D. Mcneall (2014), Is the 2004–2012 reduction of the Atlantic meridional overturning circulation significant?, *Geophys. Res. Lett.*, *41*, 3204–3210, doi:10.1002/2014GL059473.

Schmittner, A., M. Latif, and B. Schneider (2005), Model projections of the North Atlantic thermohaline circulation for the 21st century assessed by observations, *Geophys. Res. Lett.*, *32*, L23710, doi:10.1029/2005GL024368.

Shepherd, A., et al. (2012), A reconciled estimate of ice sheet mass balance, *Science*, *338*(6111), 1183–1189, doi:10.1126/science.1228102.

Sutton, R. T., and B. Dong (2012), Atlantic Ocean influence on a shift in European climate in the 1990s, *Nat. Geosci.*, *5*(11), 788–792, doi:10.1038/ngeo1595.

Sutton, R. T., and D. L. R. Hodson (2005), Atlantic Ocean forcing of North American and European summer climate, *Science*, *309*(5731), 115–118, doi:10.1126/science.1109496.

Swingedouw, D., P. Braconnot, and O. Marti (2006), Sensitivity of the Atlantic Meridional Overturning Circulation to the melting from northern glaciers in climate change experiments, *Geophys. Res. Lett.*, *33*, L07711, doi:10.1029/2006GL025765.

Swingedouw, D., C. B. Rodehacke, S. M. Olsen, M. Menary, Y. Gao, U. Mikolajewicz, and J. Mignot (2014), On the reduced sensitivity of the Atlantic overturning to Greenland ice sheet melting in projections: A multi-model assessment, *Clim. Dyn.*, *44*(11–12), 3261–3279, doi:10.1007/s00382-014-2270-x.

Tedesco, M., and X. Fettweis (2012), 21st century projections of surface mass balance changes for major drainage systems of the Greenland ice sheet, *Environ. Res. Lett.*, *7*(4), 45405, doi:10.1088/1748-9326/7/4/045405.

Van Angelen, J. H., M. R. van den Broeke, B. Wouters, and J. T. M. Lenaerts (2013a), Contemporary (1960–2012) evolution of the climate and surface mass balance of the Greenland ice sheet, *Surv. Geophys.*, *35*(5), 1155–1174, doi:10.1007/s10712-013-9261-z.

Van Angelen, J. H., J. T. M. Lenaerts, M. R. Van Den Broeke, X. Fettweis, and E. Van Meijgaard (2013b), Rapid loss of firn pore space accelerates 21st century Greenland mass loss, *Geophys. Res. Lett.*, *40*, 2109–2113, doi:10.1002/grl.50490.

Van As, D., et al. (2014), Increasing meltwater discharge from the Nuuk region of the Greenland ice sheet and implications for mass balance (1960–2012), *J. Glaciol.*, *60*(220), 314–322.

van den Berk, J., and S. Drijfhout (2014), A realistic freshwater forcing protocol for ocean-coupled climate models, *Ocean Model.*, *81*, 36–48, doi:10.1016/j.ocemod.2014.07.003.

Vizcaíno, M., U. Mikolajewicz, M. Gröger, E. Maier-Reimer, G. Schurgers, and A. M. E. Winguth (2008), Long-term ice sheet-climate interactions under anthropogenic greenhouse forcing simulated with a complex Earth System Model, *Clim. Dyn.*, *31*(6), 665–690, doi:10.1007/s00382-008-0369-7.

Vizcaíno, M., W. H. Lipscomb, W. J. Sacks, J. H. Van Angelen, B. Wouters, and M. R. Van Den Broeke (2013), Greenland surface mass balance as simulated by the Community Earth System model. Part I: Model evaluation and 1850–2005 results, *J. Clim.*, *26*(20), 7793–7812, doi:10.1175/JCLI-D-12-00615.1.

Vizcaíno, M., U. Mikolajewicz, F. Ziemen, C. B. Rodehacke, R. Greve, and M. R. van den Broeke (2015), Coupled simulations of Greenland ice sheet and climate change up to AD 2300, *Geophys. Res. Lett.*, *42*, 3927–3935, doi:10.1002/2014GL061142.

Weaver, A. J., J. Sedácek, and M. Eby (2012), Stability of the Atlantic meridional overturning circulation: A model intercomparison, *Geophys. Res. Lett.*, *39*, L20709, doi:10.1029/2012GL053763.

Weijer, W., M. E. Maltrud, M. W. Hecht, H. A. Dijkstra, and M. A. Kliphuis (2012), Response of the Atlantic Ocean circulation to Greenland Ice Sheet melting in a strongly-eddying ocean model, *Geophys. Res. Lett.*, *39*, L09606, doi:10.1029/2012GL051611.

Wouters, B., D. Chambers, and E. J. O. Schrama (2008), GRACE observes small-scale mass loss in Greenland, *Geophys. Res. Lett.*, *35*, L20501, doi:10.1029/2008GL034816.

Wouters, B., J. L. Bamber, M. R. van den Broeke, J. T. M. Lenaerts, I. Sasgen, B. Wouters, and M. V. D. Broeke (2013), Limits in detecting acceleration of ice sheet mass loss due to climate variability, *Nat. Geosci.*, *6*(8), 613–616, doi:10.1038/ngeo1874.

Yi, S., W. Sun, K. Heki, and A. Qian (2015), An increase in the rate of global mean sea level rise since 2010, *Geophys. Res. Lett.*, *42*, 3998–4006, doi:10.1002/2015GL063902.